Lensless focusing with subwavelength resolution by direct synthesis of the angular spectrum

Stanley S. Hong,[a] Berthold K. P. Horn, and Dennis M. Freeman
Department of Electrical Engineering and Computer Science, Massachusetts Institute of Technology, Cambridge, Massachusetts 02139

Michael S. Mermelstein
Lightwave Instruments, LLC, Watertown, Massachusetts 02472

(Received 17 January 2006; accepted 5 April 2006)

We consider the coherent superposition of unfocused wave fronts for lensless focusing of electromagnetic waves with subwavelength resolution. Near the focal point, intensity distributions generated using the approach approximate those generated using lenses. Far from the focal point, discretization of spatial frequencies results in a trade-off between the number of wave fronts and the accuracy of the approximation. We experimentally demonstrate the feasibility of the approach by generating an approximation of an azimuthally polarized Bessel beam with a focal spot diameter (full width at half maximum intensity) of 0.37λ. © *2006 American Institute of Physics*.
[DOI: 10.1063/1.2213912]

The ability to focus electromagnetic waves with subwavelength resolution is essential to a wide range of applications including microscopy, semiconductor lithography, and optical trapping. Focusing is most commonly accomplished using refractive lenses, and lenses with resolutions limited only by diffraction are ubiquitous. However, there are instances where focusing with lenses is difficult or not feasible. For example, focusing with subwavelength resolution is technically challenging in the x-ray, ultraviolet, and infrared regions of the spectrum, due largely to the lack of suitable refractive materials. Alternate approaches employed in these regions of the spectrum have included reflective lenses[1–3] and diffractive Fresnel zone plates,[4,5] and more recent approaches include capillary optics,[6,7] compound refractive lenses,[8] and photon sieves.[9]

An intriguing approach to focusing electromagnetic waves is the coherent superposition of unfocused wave fronts. This approach has been proposed in several contexts including optical phased-array beam steering,[10,11] phase-locked laser arrays,[12,13] and coherent combination of single-mode optical fibers.[14,15] In the context of focusing with subwavelength resolution, the approach offers numerous important advantages. In particular, the approach can be implemented entirely using flat mirrors (i.e., refractive materials are not required). Also, resolution is not affected by lens aberrations. Further, since the phase of each wave front is independently modulated, subwavelength accuracy is not required in the construction of the apparatus.

In this letter we consider the coherent superposition of unfocused wave fronts for focusing electromagnetic waves with subwavelength resolution. The approach can be understood using the "angular spectrum of plane waves" concept. The angular spectrum of plane waves concept asserts that any propagating monochromatic field can be represented as a superposition of homogeneous and inhomogeneous (i.e., evanescent) plane waves.[16] In the scalar approximation of electromagnetic wave theory, the directions, amplitudes, and phases of the plane waves are related to the field by a Fourier transform. The elegance of this approach is a hallmark of Fourier optics.[17] Angular spectrum decomposition is well understood and widely used for analysis.[18] It is not as widely recognized, however, that the angular spectrum concept can also be used for synthesis: A focused beam can be synthesized directly from its angular spectrum of plane waves.

Direct synthesis of the angular spectrum is illustrated conceptually in Fig. 1. In general, the angular spectrum of a focused beam is described by a continuous function. Figure 1(b) shows a Bessel beam which has an intensity distribution described by $I(r)=J_0^2(k_r r)$, where r is a cylindrical coordinate (i.e., $r=\sqrt{x^2+y^2}$), J_0 is the zero-order Bessel function of first kind, and $k_r=(2\pi/\tilde{\lambda})$.[19,20] The angular spectrum can be synthesized using a superposition of plane waves, and the corresponding intensity distribution $I(\mathbf{r})$ can be written as

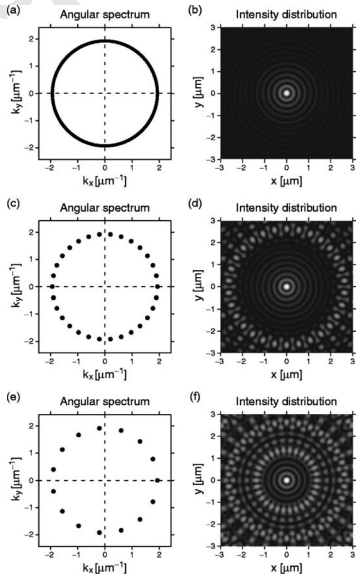

FIG. 1. Direct synthesis of the angular spectrum. (a) Angular spectrum and (b) intensity distribution of ideal Bessel beam. (c) Angular spectrum and (d) intensity distribution of synthesis using 30 plane waves. (e) Angular spectrum and (f) intensity distribution of synthesis using 15 plane waves.

[a]Electronic mail: stanhong@mit.edu

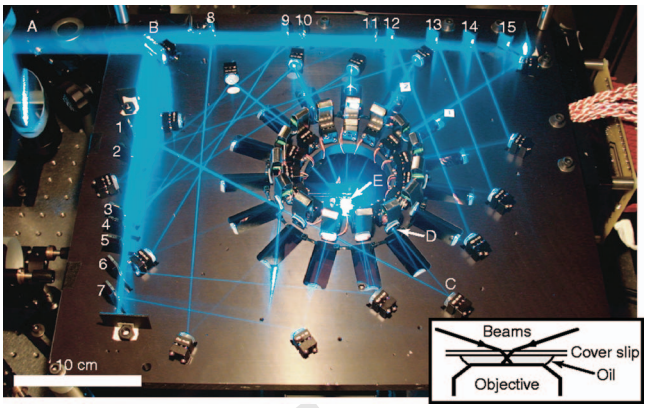

FIG. 2. (Color) Experimental apparatus for angular spectrum synthesis using 15 laser beams. The expanded beam of a visible-light laser (A) is spatially chopped in half by a mirror (B) and then further chopped into 15 beams by two rows of pick-off mirrors (1–7 and 8–15). Each of the 15 beams is then directed by a subsequent mirror (C) to one of a ring of 15 mirrors (D), each mounted on a piezoelectric actuator. The actuated mirrors then direct the beams down through a ring of slots to a final ring of recessed mirrors, which direct the beams to a common region of overlap (E). In the region of overlap, the converging cone of 15 beams passes through a cover slip into immersion oil (inset illustrates cross section), where the intensity distribution at the focal plane of a high-power oil-immersion objective is imaged.

$$I(\mathbf{r}) = \frac{1}{2}\left[\sum_{n=1}^{N} \mathbf{E}_n \exp(i\mathbf{k}_n \cdot \mathbf{r})\right] \cdot \left[\sum_{n=1}^{N} \mathbf{E}_n \exp(i\mathbf{k}_n \cdot \mathbf{r})\right]^* = \sum_{n=1}^{N} \frac{|\mathbf{E}_n|^2}{2} + \sum_{m=1}^{N-1} \sum_{n=m+1}^{N} |\mathbf{E}_m| \cdot |\mathbf{E}_n| \tag{1}$$

$$\times \cos[(\mathbf{k}_m - \mathbf{k}_n) \cdot \mathbf{r} + (\angle \mathbf{E}_m - \angle \mathbf{E}_n)], \tag{2}$$

where $\mathbf{r}$ is a position vector (i.e., $\mathbf{r}=\hat{\mathbf{x}}x+\hat{\mathbf{y}}y+\hat{\mathbf{z}}z$), N is the number of plane waves, $\mathbf{E}_n$ and $\mathbf{k}_n$ denote, respectively, the complex electric-field vector and wave vector of the nth plane wave, $|\cdot|$ denotes complex modulus, and $\angle$ denotes complex phase.[21] If the angular spectrum of a Bessel beam [Fig. 1(a)] is synthesized using a finite number of plane waves [Figs. 1(c) and 1(e)], the corresponding intensity distributions approximate the ideal focused beam in a circular region centered at the focal point and delineated by a ring of "synthesis artifacts" [Figs. 1(d) and 1(f)].[22] The radius of the region is approximately $N\tilde{\lambda}/(2\pi)$.

The theoretical predictions and feasibility of the approach were verified using the experimental apparatus shown in Fig. 2. The apparatus converts the expanded linearly polarized beam of an argon ion laser (λ=488 nm) into a converging circular cone of 15 beams with a half angle of 72° [numerical aperture (NA)=0.95]. Beam paths were designed with matching path lengths, and mirrors were mounted on a single aluminum plate for mechanical and thermal stabilities. One mirror in each beam path was mounted on a piezoelectric actuator, allowing the phase of each beam to be modulated independently. With the exception of a beam expander (not shown), the optical path consists entirely of flat mirrors.

The intensity distribution generated by the apparatus was measured by projecting the cone of beams through a glass cover slip and into the oil-immersed focal plane of a 160 ×/1.4 NA oil-immersion microscope objective. The magnified image produced by the objective was recorded with a charge-coupled device (CCD) imager. In general, the intensity distribution generated by a high-NA focused beam cannot be measured accurately in this manner due to the effects of polarization: The electric-field vectors of the radially polarized component are rotated by the microscope objective. However, the field generated by the apparatus was designed to be azimuthally polarized.[23] As a result, the intensity distribution incident on the CCD imager was simply a magnified replica of the intensity distribution at the focal plane of the objective.

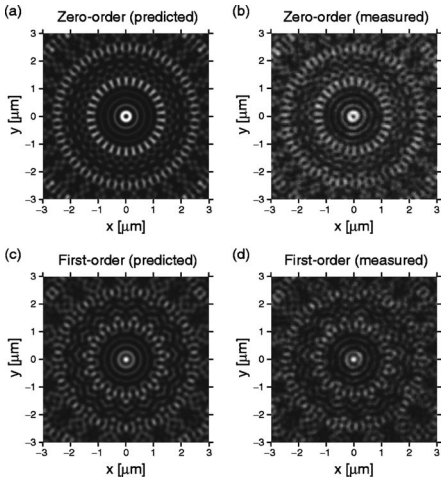

FIG. 3. Intensity distributions generated by the experimental apparatus. (a) Predicted and (b) measured zero-order Bessel-beam approximation. (c) Predicted and (d) measured first-order Bessel-beam approximation.

While the design of the beam paths correctly sets the polarization and wave vectors of the 15 beams, generating a focused beam also requires that the beam amplitudes and phases are equal at the focal point. Since the transverse amplitude profile of each beam was smoothly varying but nonconstant, the amplitudes were matched by suitable lateral adjustments of the beams. The phases were not as straightforward to adjust, as it was not possible to measure the phases of the beams directly. Since we could measure the intensity distribution generated by the apparatus, we developed a method for estimating the relative beam phases from the pattern (see below). Each piezoelectric phase actuator was then adjusted accordingly to achieve the desired phase relation amongst the beams.

Figures 3 and 4 show the predicted and measured intensity distributions generated by the apparatus. With the beam phases equal at the focal point, the apparatus generates a 15-plane-wave approximation of an azimuthally polarized zero-order Bessel beam.[28,29] The predicted [Fig. 3(a)] and measured [Fig. 3(b)] intensity distributions feature an annu-

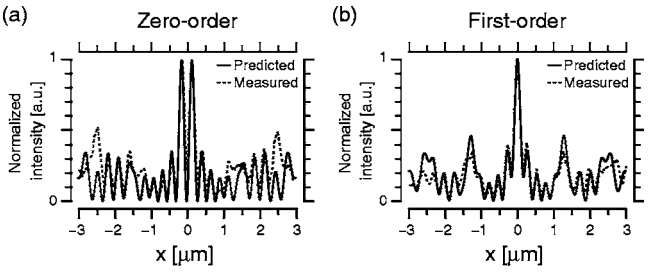

FIG. 4. Intensity distributions generated by the experimental apparatus. (a) Cross sections through centers of Figs. 3(a) and 3(b). (b) Cross sections through centers of Figs. 3(c) and 3(d).

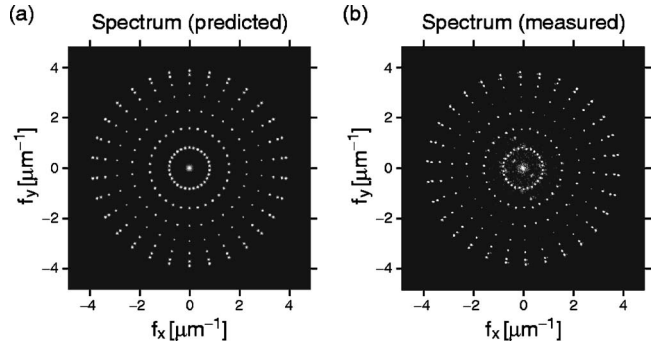

FIG. 5. Intensity spectra generated by the experimental apparatus. (a) Fourier transform of Fig. 3(a). (b) Fourier transform of Fig. 3(b). Complex magnitude is shown on a logarithmic gray scale.

lus approximately 280 nm in diameter and a ring of synthesis artifacts approximately 1.2 μm in radius. Alternatively, with each beam phase set to the azimuthal angle of the beam, the apparatus generates the corresponding approximation of a first-order Bessel beam. The predicted [Fig. 3(c)] and measured [Fig. 3(d)] intensity distributions feature a focal spot approximately 180 nm in full width at half maximum diameter and a ring of synthesis artifacts approximately 1.2 μm in radius. The axial structure of the intensity distribution was investigated by translating the microscope objective along the optical axis; over an axial distance of 50 μm, the transverse size of the focal spot increased from 180 to 210 nm in diameter.

Figure 5 shows the Fourier transform of the predicted and measured intensity distributions.[30] The predicted intensity spectrum can be calculated by taking the Fourier transform of both sides of Eq. (1) and can be simplified by

$$\mathcal{F}\{I(\mathbf{r})\} = \frac{1}{2}\left\{\left[\sum_{n=1}^{N}\mathbf{E}_n\delta(\mathbf{f}-\mathbf{k}_n)\right]\star\left[\sum_{n=1}^{N}\mathbf{E}_n\delta(\mathbf{f}-\mathbf{k}_n)\right]\right\}, \tag{3}$$

where $\mathbf{f}$ is a spatial-frequency vector (i.e., $\mathbf{f}=\hat{\mathbf{x}}f_x+\hat{\mathbf{y}}f_y+\hat{\mathbf{z}}f_z$) and $\star$ denotes three-dimensional cross correlation. The measured intensity spectrum [Fig. 5(b)] is well fitted by the autocorrelation of a ring of impulses, as predicted by Eq. (3). The irregularity in the amplitudes of the impulses in the measured intensity spectrum can be attributed to unequal beam amplitudes, while deviations in the locations of the impulses can be attributed to errors in the orientations of the beams.

To conclude, we have considered both theoretically and experimentally a lensless approach to focusing electromagnetic waves with subwavelength resolution. The approach can be implemented entirely using reflective elements and does not require subwavelength accuracy in the construction of the apparatus. Intensity distributions generated using the approach approximate those generated using lenses near the focal point and are strikingly characterized by a discretization of spatial frequencies.

The Fourier transform of $I(\mathbf{r})$ can be expressed as a summation of impulses [Eq. (3)]. Each impulse corresponds to a pair of plane waves (e.g., plane waves m and n); the location and complex amplitude of each impulse are given by $\mathbf{k}_m-\mathbf{k}_n$ and $\mathbf{E}_m\cdot\mathbf{E}_n^*$, respectively. If all the wave vectors $\mathbf{k}_n$ are known, the complex amplitude $\mathbf{E}_m\cdot\mathbf{E}_n^*$ for every pair of plane waves can be determined from $\mathcal{F}\{I(\mathbf{r})\}$. Subsequently, if $\mathbf{E}_m\cdot\mathbf{E}_n^*$ for every pair of plane waves is known, the complex amplitude of every plane wave $\mathbf{E}_n$ is overdetermined. Hence, the amplitudes and phases of all the plane waves can be determined from an image of the intensity distribution $I(\mathbf{r})$.

Our method consists of three steps. The first step estimates $\mathbf{k}_n$ from $I(\mathbf{r})$ using a Fourier transform followed by a matched Hough transform. The intensity distribution $I(\mathbf{r})$ is first multiplied by a circularly symmetric raised-cosine window, and then $\mathcal{F}\{I(\mathbf{r})\}$ is estimated using the two-dimensional fast Fourier transform. The complex magnitude of $\mathcal{F}\{I(\mathbf{r})\}$ is shown in Fig. 5(b).[30] Since the wave vectors in our experimental apparatus were arranged in a circular cone, the angular spectrum $\Sigma_{n=1}^{N}\mathbf{E}_n\delta(\mathbf{f}-\mathbf{k}_n)$ consisted of impulses arranged in a circle. Since $\mathcal{F}\{I(\mathbf{r})\}$ is the autocorrelation of the angular spectrum [Eq. (3)], $\mathbf{k}_n$ can be estimated using a matched Hough transform by replacing each pixel in $\mathcal{F}\{I(\mathbf{r})\}$ with the line integral around a circle centered at that pixel. The radius of the circle is approximately half the radius of the largest ring of impulses in $\mathcal{F}\{I(\mathbf{r})\}$. The matched Hough transform contains a ring of $2N$ peaks from which $\mathbf{k}_n$ can be estimated.

The second step in our method estimates $\mathbf{E}_m\cdot\mathbf{E}_n^*$ for every pair of plane waves from $\mathbf{k}_n$ (estimated in the first step) and $\mathcal{F}\{I(\mathbf{r})\}$. The impulse in $\mathcal{F}\{I(\mathbf{r})\}$ with complex amplitude $\mathbf{E}_m\cdot\mathbf{E}_n^*$ should be located at spatial frequency $\mathbf{k}_m-\mathbf{k}_n$. Since the impulses were well resolved in $\mathcal{F}\{I(\mathbf{r})\}$ [Fig. 5(b)], $\mathbf{E}_m\cdot\mathbf{E}_n^*$ was estimated as the complex value of the pixel with the largest complex modulus in the 11×11-pixel region of $\mathcal{F}\{I(\mathbf{r})\}$ centered at $\mathbf{k}_m-\mathbf{k}_n$. Note that while Eq. (3) can be written as the sum of N^2 impulses, N of the impulses corresponds to the same spatial frequency (i.e., $\mathbf{k}_m-\mathbf{k}_n=0$ for all $m=n$). As a result, $\mathcal{F}\{I(\mathbf{r})\}$ contains at most N^2-N+1 distinct impulses corresponding to the sum of a zero-frequency term and ${}_NP_2=N(N-1)$ interference terms.

The third step in our method estimates the complex amplitude $\mathbf{E}_n$ of every plane wave from $\mathbf{E}_m\cdot\mathbf{E}_n^*$ for every pair of plane waves (estimated in the second step). An error function can be defined as

$$E(\mathbf{X}_1,\ldots,\mathbf{X}_N) = \sum_{m=1}^{N}\sum_{n=1}^{N}|\mathbf{E}_m\cdot\mathbf{E}_n^*-\mathbf{X}_m\cdot\mathbf{X}_n^*|, \tag{4}$$

where $\mathbf{E}_m\cdot\mathbf{E}_n^*$ are the *observed* complex amplitudes (estimated in the second step) and $\mathbf{X}_n$ is the *unknown* complex amplitude of the nth plane wave. Since N unknown amplitudes $\mathbf{X}_n$ are constrained by up to N^2-N+1 observations of $\mathbf{E}_m\cdot\mathbf{E}_n^*$, $\mathbf{X}_n$ is overdetermined and can be estimated by minimizing the error function. The initial guesses for the amplitudes, phases, and directions of $\mathbf{X}_n$ were identically unity, random with uniform distribution between 0 and 2π radians, and orthogonal to $\mathbf{k}_n$ (estimated in the first step) assuming perfect azimuthal polarization, respectively. On average, an iterative technique developed for minimizing the error function settled to less than 0.1% change between iterations after 4.7 iterations.

The authors acknowledge H. I. Smith, P. T. C. So, J. M. Fini, C. C. Abnet, A. J. Aranyosi, S. Desai, J. Ryu, and J. W. Gu for their contributions. This work was supported by the Defense Advanced Research Projects Agency (DARPA) under Grant No. N66001-00-1-8908.

[1]K. Schwarzschild, Astron. Mittheil. der Königl. Sternwarte Götingen **10**, 3 (1905).

[2]P. Kirkpatrick and A. V. Baez, J. Opt. Soc. Am. **38**, 766 (1948).
[3]H. Wolter, Ann. Phys. **10**, 94 (1952).
[4]A. V. Baez, Nature (London) **186**, 958 (1960).
[5]D. Attwood, *Soft X-rays and Extreme Ultraviolet Radiation: Principles and Applications* (Cambridge University Press, Cambridge, 1999).
[6]M. A. Kumakhov, Nucl. Instrum. Methods Phys. Res. B **48**, 283 (1990).
[7]D. H. Bilderback and D. J. Thiel, Rev. Sci. Instrum. **66**, 2059 (1995).
[8]A. Snigirev, V. Kohn, I. Snigireva, and B. Lengeler, Nature (London) **384**, 49 (1996).
[9]L. Kipp, M. Skibowski, R. L. Johnson, R. Berndt, R. Adelung, S. Harm, and R. Seemann, Nature (London) **414**, 184 (2001).
[10]R. A. Meyer, Appl. Opt. **11**, 613 (1972).
[11]D. P. Resler, D. S. Hobbs, R. C. Sharp, L. J. Friedman, and T. A. Dorschner, Opt. Lett. **21**, 689 (1996).
[12]D. R. Scifres, R. D. Burnham, and W. Streifer, Appl. Phys. Lett. **33**, 1015 (1979).
[13]J. Katz, S. Margalit, and A. Yariv, Appl. Phys. Lett. **42**, 554 (1983).
[14]G. Josten, H. P. Weber, and W. Luethy, Appl. Opt. **28**, 5133 (1989).
[15]M. Tempus, W. Luthy, and H. P. Weber, Appl. Phys. B: Photophys. Laser Chem. **56**, 79 (1993).
[16]L. Mandel and E. Wolf, *Optical Coherence and Quantum Optics* (Cambridge University Press, Cambridge, 1995).
[17]J. W. Goodman, *Introduction to Fourier Optics*, 2nd ed. (McGraw-Hill, New York, 1996).
[18]*Selected Papers on Scalar Wave Diffraction*, edited by K. E. Oughstun (SPIE, Bellingham, WA, 1992).
[19]J. Durnin, J. Opt. Soc. Am. A **4**, 651 (1987).
[20]For clarity, we define $\tilde{\lambda}=\lambda/\mathrm{NA}$, where λ is wavelength and NA is numerical aperture.
[21]G. Bekefi and A. H. Barrett, *Electromagnetic Vibrations, Waves, and Radiation* (MIT, Cambridge, MA, 1977).
[22]The effects of polarization are neglected in Fig. 1 for simplicity.
[23]The generation of azimuthally and radially polarized fields using the coherent superposition of linearly polarized fields is well known (Ref. 24), and various alternate techniques are described in the literature (Refs. 25–27).
[24]S. C. Tidwell, D. H. Ford, and W. D. Kimura, Appl. Opt. **29**, 2234 (1990).
[25]D. Pohl, Appl. Phys. Lett. **20**, 266 (1972).
[26]R. Oron, S. Blit, N. Davidson, A. A. Friesem, Z. Bomzon, and E. Hasman, Appl. Phys. Lett. **77**, 3322 (2000).
[27]U. Levy, C.-H. Tsai, L. Pang, and Y. Fainman, Opt. Lett. **29**, 1718 (2004).
[28]R. H. Jordan and D. G. Hall, Opt. Lett. **19**, 427 (1994).
[29]Z. Bouchal and M. Olivík, J. Mod. Opt. **42**, 1555 (1995).
[30]Note that Fig. 5(b) was calculated using the full 1024×1024-pixel region recorded with the CCD imager, while Figs. 3(b) and 3(d) show a 128×128-pixel detail.